The Spatial Variations of Urban Land Surface Temperatures: Pertinent Factors, Zoning Effect, and Seasonal Variability

Qihao Weng, *Member, IEEE*, Hua Liu, Bingqing Liang, and Dengsheng Lu

***Abstract*—Remote sensing of urban land surface temperatures (LST) has been conducted based largely on pixel-by-pixel correlation with land use and land cover (LULC) types. Few studies have examined the spatial variations of LST within land use zoning polygons, in spite of its significance on the knowledge of environmental implications or planning practices. This study aimed to analyze the spatial patterns of LSTs and to explore factors contributing to the LST variations in the city of Indianapolis. Four Terra's ASTER images, representing distinct seasons, were used in conjunction with other types of spatial data for the analysis. The potential factors were grouped into the categories of LULC composition, biophysical conditions, intensity of human activities, and landscape pattern. Statistical analyses were conducted to determine the relative importance of each group of the variables. Moreover, the spatial variations of LST were examined at both the residential and general zoning levels, so that the environmental effect of urban planning on LST may be assessed. By analyzing the mean and standard deviation values of normalized LSTs, the seasonal dynamics of LST were finally studied. Results show that the biophysical variables were most significant in explaining the spatial variations of LST. At both zoning levels, LST possessed a weaker relationship with the LULC compositions than with the biophysical variables. Principal component analysis further indicates that the cumulative variance was always larger in residential zoning, implying that the factors contributing to the LST variations in general zoning might be more complex than those for the residential zoning. An interesting finding of this study was in the relationship between LST and the landscape metrics of zoning polygons. It suggests that smaller residential zoning polygons were associated with larger temperature variations, and that the more complex in shape a residential zoning category was, the more intrapolygon variation of LST tended to be. These correlations, however, did not exist in the nonresidential zoning categories. The spatial pattern of LST in Indianapolis may be characterized as concentric in the central part of the city, a hot ring along the Highway 465, and several hot corridors along the radial highways outward to the countryside. The seasonal fluctuation of LST was weak in the central part, but increased towards the countryside. Due to the amount of anthropogenic heat, land use zones with less human activities were found to have a strong seasonal variability, whereas the zones with intensive human activities fluctuated less in LST.**

***Index Terms*—Environmental impact, land use zoning, seasonal variability, spatial pattern, urban land surface temperature.**

I. Introduction

URBAN land surface temperature (LST) pattern is a manifestation of surface energy balance, and has been extensively studied with thermal remote sensing technology. LST are regarded as a function of four surface and subsurface properties: albedo, emissivity, the thermal properties of urban construction materials (including moisture), and the composition and structure of urban canopy [1]. Because the receipt and loss of radiation of urban surfaces correspond closely to the distribution of land use and land cover (LULC) characteristics [2], [3], there has been a tendency to use thematic LULC data, not quantitative surface descriptors, to describe urban thermal landscapes [4]. This trend of qualitative description of thermal patterns and simple correlations between LULC types and their thermal signatures has slowed down the development of remote sensing of LST and, thus, surface temperature heat islands [4]. To study urban LST, some sophisticated numerical and physical models have been developed. These include energy balance models, by far the main methods, [5], [6], laboratory models [7], 3-D simulations [8], Gaussian models [9], and other numerical simulations. Estimation of surface energy fluxes has been conducted by using medium- resolution satellite imagery, such as Landsat TM/ETM+ and ASTER imagery. Zhang *et al.* used Landsat TM data, in combination with routine meteorological data and field measurements, to estimate the urban surface energy fluxes in Osaka, Japan, and to analyze their spatial variability in both summer and winter seasons [10]. Chrysoulakis used ASTER imagery to determine the spatial distribution of all-wave surface net radiation balance in Athens, Greece [11]. Kato and Yamaguchi combined ASTER and Lansat ETM+ data to investigate the spatial patterns of surface energy fluxes in Nagoya, Japan, in four seasons [12]. Statistical analysis may play an important role in linking LST to related factors, especially at large scales. Previous studies have focused primarily on biophysical and meteorological factors, such as built-up area and height [13], urban and street geometry [14], LULC [3], [15], and vegetation. The relationship between LST and vegetation cover has been extensively studied by using vegetation indices such as NDVI [2], [3], [16]–[18]. However, the relationship between NDVI and

Manuscript received August 16, 2007. First published September 30, 2008; current version published October 15, 2008. This work was supported by grants from the National Science Foundation (BCS-0521734) and the Indiana State University Research Committee (UNR267).

Q. Weng and B. Liang are with the Department of Geography, Center for Urban and Environmental Change, Indiana State University, Terre Haute, IN 47809 USA (e-mail: qweng@indstate.edu).

H. Liu is with the Department of Political Science and Geography, Old Dominion University, Norfolk, VA 23529 USA.

D. Lu is with the School of Forestry and Wildlife Sciences, Auburn University, Auburn, AL 36849 USA.

Color versions of one or more of the figures in this paper are available online at http://ieeexplore.ieee.org.

Digital Object Identifier 10.1109/JSTARS.2008.917869

fractional vegetation cover is not singular. Weng *et al.* found that LST possessed a slightly stronger negative correlation with vegetation fraction derived from a spectral mixture modeling, than with NDVI for all LULC types across the spatial resolution ranging from 30 to 960 m [19].

Previous researches have focused more on the relationship between LST variation, and the thermal properties and composition of urban construction materials, than the effect of urban morphology and its component surfaces. Oke suggested that each component surface in urban landscapes (e.g., lawn, parking lot, road, building, cemetery, and garden) exhibits a unique radiative, thermal, moisture, and aerodynamic properties, and relates to their surrounding site environment [20]. The myriad of the component surfaces and the spatial complexity of their mosaic create a limitless array of microclimate systems, preventing any generalization [20]. The microscale of the urban morphological characteristics renders it difficult to analyze the LST variation using the energy budget approach. Remote sensing derived biophysical attributes provide great potentials to parameterize urban construction materials and the composition and structure of urban canopies, and for linking with pixel-based LST measurements in understanding of the surface energy budget and the urban heat island (UHI) phenomenon. Recent advancement in landscape ecology has facilitated the characterization of urban surface components and their quantitative links to environmental processes (e.g., the UHI process).

This research examines the relationship between the spatial variations of LST and the composition and structure of urban surface. Four ASTER images, one for each season, over the city of Indianapolis are used in conjunction with other types of spatial data for the analysis. Specific objectives of this research are to analyze the spatial patterns of LSTs and to explore factors that have contributed to the LST variations. The potential factors are grouped into four categories, i.e., LULC composition, biophysical conditions, intensity of human activities, and landscape pattern. Statistical analysis is conducted to determine the relative importance of each group of the variables. Moreover, by employing satellite images of different seasons, the dynamics of the LST and its interaction with the explanatory factors may be investigated. Finally, the spatial variations of LST are examined in both levels of residential and general zoning to assess the environmental implications of urban planning.

II. Study Area

The City of Indianapolis, located in Marion County, Indiana, is the twelfth largest city in United States, with approximately 0.8 million population (over 1.6 million in the metropolitan area). Indianapolis is located on a flat plain, and is relatively symmetrical, having possibilities of expansion in all directions. The areal expansion is through encroachment into the adjacent agricultural and nonurban land. Certain decision-making forces have encouraged some sectors of Metropolitan Indianapolis to expand faster than others. Detecting and analyzing its urban thermal landscape is significant to control and plan the city's future development and to monitor the environmental impacts of urbanization. The city has a temperate climate without pronounced wet or dry seasons. However, obvious seasonal changes can be found in the area. Its annual average air temperature is 52.3 °F, and the average temperature in January reaches 26.0 °F and 75.0 °F in July. The average annual precipitation is 39.9 in, and about 2.3 in in January and 4.6 in in July. The average wind speeds are slightly higher in spring and winter than in summer and fall seasons. The average relative humidity for the whole year does not show obvious seasonal changes. The synoptic weather conditions during the satellite acquisitions were typical for the study area for each respective season. Our previous research suggests that LST variations and their relationships with urban surface materials varied with images acquired in different times of the year [21], which prompts us to examine systematically the seasonality of LST spatial variability in this study.

III. Methods

A. Image Preprocessing

ASTER images, acquired on October 3, 2000 (fall), June 25, 2001 (summer), April 5, 2004 (spring), and February 6, 2006 (winter), respectively, were used in this research. ASTER data have 14 bands with different spatial resolutions, i.e., two visible bands and one near infrared (VNIR) band with 15-m spatial resolution, six shortwave infrared (SWIR) bands with 30-m spatial resolution, and five thermal infrared (TIR) bands with 90-m spatial resolution. The level 1B ASTER data were purchased, which consisted of the image data, radiance conversion coefficients, and ancillary data [22]. Although these ASTER images have been radiometrically and geometrically corrected, however, the root mean square error (RMSE) were so large that they could not meet our research needs. We conducted a geometric correction for each image, using 1:24000 USGS digital raster graphs (DRG) as reference maps. At least 30 ground control points were selected for each georectification, and the nearest neighbor resampling method was applied with the pixel size of 15 m for all VNIR, SWIR, and TIR bands. The RMSE of less than 0.5 pixel was achieved for all georectifications.

B. Land Use and Land Cover Classification

1) Definition of Land Cover and Land Use Classes: Land use and land cover (LULC) maps were produced with an unsupervised classification algorithm called Iterative Self-Organizing Data Analysis (ISODATA). The images (VNIR and SWIR bands) were classified into six LULC types, including agricultural land, aquatic systems, barren land, developed land, forest land, and grassland. Agricultural land is characterized by herbaceous vegetation that has been planted or is intensively managed for the production of food. This category includes croplands such as corn, wheat, soybean, and cotton, and also includes fallow land. Aquatic systems refer to all areas of open water, including lake, rivers and streams, ponds, and outdoor swimming pools. Barren lands are the areas that characterized by bare rock, gravel, sand, silt, clay, or other earthen material and no green vegetation present, including quarries, bare dune, construction sites, and mine. Developed lands are defined as the areas that have a high percentage (30 percent or greater) of constructed materials, such as asphalt, concrete, and buildings. This category includes commercial, industrial, transportation, and low and high residential uses. Forest lands are the areas

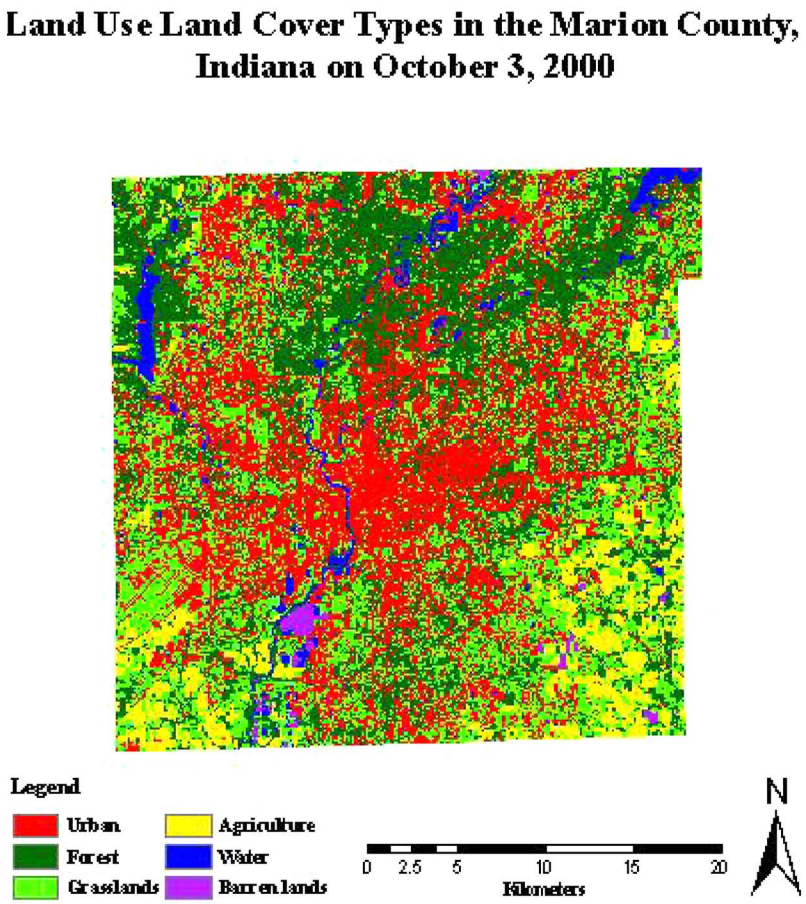

Fig. 1. LULC map of Marion County, Indiana, on October 3, 2000.

characterized by tree cover (natural or semi-natural woody vegetation), including natural deciduous forest, evergreen forest, mixed forest, urban and suburban forest, and shrubs. Grasslands refer to the areas covered by herbaceous vegetation including pasture/hay planted for livestock grazing or the production of hay. It also includes the urban/recreational grasses—planted in developed settings for recreation, erosion control, or aesthetic purposes, such as parks, lawns, golf courses, airport grasses, and industrial site grasses.

2) Image Classification Procedure: Remotely sensed data are often highly correlated between the adjacent spectral wavebands, and redundant bands would slow down the image processing if all bands were used. Principal component analysis was applied to identify which bands out of the nine VNIR and SWIR bands would contain more information. Based on the correlation coefficients between the bands and the first component, 5–6 bands would normally selected for classification. Because the visible (green and red) and near infrared bands were found useful in all cases, these three bands were always used in the image classifications.

Due to the complexity of LULC types in the study area, each image scene was first stratified into two sub-scenes, one for the urban area and the other for surrounding rural area. Image classification was performed separately for each sub-scene, and the results were then merged. Fifty spectral clusters were generated with ISODATA. Next, spectral classes were labeled after referencing to high-resolution aerial photographs and other geospatial data. After the first unsupervised classification, if we could not label all spectral classes, we would then mask out those confused classes and run a second unsupervised classification. The same procedure would repeat for a third classification if confusion still existed after the second classification.

Accuracy assessment of classification images were conducted by using an error matrix. Some important measures, such as overall accuracy, producer's accuracy, and user's accuracy, can be calculated from the error matrix. In this study, a total of 350 points were checked on each classified image using a stratified random sampling method. Digital orthophotos of 2003 were used as the reference data. The color orthophotographs were provided by the Indianapolis Mapping and Geographic Infrastructure System, which was acquired in April 2003 for the entire county. The orthophotographs had a spatial resolution of 0.14 m. The coordinate system belonged to Indiana State Plane East, Zone 1301, with North American Datum of 1983. The orthophotographs were re-projected and re-sampled to 1-m pixel size for the sake of quicker display and shorter computing time. The overall classification accuracy of 87% (Oct. 3, 2002, image), 88.33% (June 16, 2001, image), 92% (April 5, 2004, image), and 87.33% (February 6, 2006, image) was achieved, respectively. Fig. 1 shows the resultant classified LULC map in October 3, 2002. We further made a comparison among the four classified maps to ensure con-

TABLE I
VARIABLES APPLIED TO EXAMINE LST VARIATIONS

Categories of Variables	Variables	Meaning of Variables
LULC Composition	Per_Ur	Percentage of built-up land
	Per_Ba	Percentage of barren land
	Per_Gr	Percentage of grassland
	Per_Ag	Percentage of agricultural land
	Per_Fo	Percentage of forest land
	Per_Wa	Percentage of water bodies
Biophysical Conditions	NDVI	Mean value of Normalized Difference Vegetation Index
	GV	Mean value of green vegetation fraction derived from SMA
	IMP	Mean value of impervious surface fraction derived from SMA
	SOIL	Mean value of soil fraction derived from SMA
Intensity of Human Activities	PAVEMENT	Percentage of pavement area per zoning polygon
	BLDG_ARE	Percentage of building area per zoning polygon
	MEAN_POP	Mean population in a zoning polygon
	POP_DEN	Population density in a zoning polygon
Landscape Patterns	SHAPE_IN	Shape index of a zoning polygon
	FRACTAL	Fractal dimension of a zoning polygon
	LANDSIM	Landscape similarity index (%)
	DIVERS	Shannon's diversity index of LULC composition within a zoning polygon

sistency within the classes, and found that the magnitude and spatial pattern of each class corresponded well to each other but also reflected the seasonal and temporal differences.

C. Spectral Mixture Analysis

Spectral mixture analysis (SMA) is regarded as a physically based image processing technique that supports repeatable and accurate extraction of quantitative sub-pixel information [23]–[25]. It assumes that the spectrum measured by a sensor is a linear combination of the spectra of all components within the pixel [24], [26]. In this study, SMA was used to develop green vegetation, soil, and impervious surface fraction images. End-members were initially identified from high-resolution aerial photographs. An improved image based dark object subtraction model has proved effective and was applied to reduce the atmospheric effects [27]. After the implementation of atmospheric correction and geometrical rectification of ASTER images, a constrained least-squares solution was applied to unmix the nine VNIR and SWIR bands of ASTER imagery into fraction images, including high albedo, low albedo, vegetation, and soil fractions. An impervious surface was then estimated based on the relationship between high and low albedo fractions and the impervious surfaces. For more details about the derivation of fraction images, please refer to the article by Lu and Weng [21].

D. Estimation of LST

Various algorithms have been developed for converting ASTER TIR measurements to surface kinetic temperatures (i.e., LST) as reported by the ASTER Temperature/Emissivity Working Group [28] and Gillespie *et al.* [29]. However, a universally accepted method is not available currently for computing LSTs from multiple bands of TIR data such as those found on ASTER. In this study, we selected ASTER Band 13 (10.25–10.95 μm) to compute LSTs, because the spectral width of this band is close to the peak radiation of the blackbody spectrum given off by the urban surface of the study area. Two steps were taken to compute LSTs: 1) converting spectral radiance to at-sensor brightness temperature (i.e., blackbody temperature); and 2) correcting for spectral emissivity. We adopted the most straightforward approximation to replace the sensor response function with a delta function at the sensor's central wavelength to invert LSTs with the assumption of uniform emissivity [30]–[32]. The conversion formula is

$$T_c = \frac{C_2}{\lambda_c \ln\left(\frac{C_1}{\lambda_c^5 \pi L_\lambda} + 1\right)} \tag{1}$$

where $\mathrm{T_c}$ is brightness temperature in Kelvin (K) from a central wavelength, L_λ is spectral radiance in $\mathrm{Wm^{-3}sr^{-1}\mu m^{-1}}$, λ_c is the sensor's central wavelength, C_1 is first radiation constant ($3.74151{*}10^{-16}$ $\mathrm{Wm^{-2}sr^{-1}\mu m^{-1}}$), and C_2 is the second radiation constant (0.0143879 mK).

The temperature values obtained above are referenced to a black body. Therefore, corrections for spectral emissivity (ϵ) became necessary according to the nature of land cover. Each of the land cover categories was assigned an emissivity value according to the emissivity classification scheme by Snyder *et al.* [33]. The emissivity corrected LST was computed as follows [34]:

$$\mathrm{LST} = \frac{T_c}{1 + (\lambda * T_c/\rho)\ln\epsilon} \tag{2}$$

where: $\lambda =$ wavelength of emitted radiance (for which the peak response and the average of the limiting wavelengths ($\lambda = 10.6\,\mu$m) [35], $\rho = \mathrm{h}{*}c/\sigma$ ($1.438{*}10^{-2}$ mK), $\sigma =$ Boltzmann constant (1.38 * 10^{-23} J/K), h = Planck's constant ($6.626{*}$ 10^{-34} Js), and c = velocity of light ($2.998{*}$ 10^8 m/s).

TABLE II
GENERAL ZONING (POLYGON) ATTRIBUTES

Zoning category	Code	Description	Number of polygons	Percent of landscape	Mean polygon size (ha)	Mean shape index	Mean fractal dimension
Historical Preservation	HP	historic preservation district including a variety of land uses (mostly residential)	1	0.01	8.64	1.44	1.29
Special Uses	SU	wide variety of uses such as schools, utility infrastructure, cemeteries, libraries, community centers, charitable organizations, golf courses, and penal institutions	1232	17.84	14.09	1.38	1.32
University	UQ	variety of land uses typical of higher education institutions including classroom, office, dormitory, facility maintenance, and parking structures	13	0.19	19.24	1.28	1.35
DA-Agriculture	DA	agriculture and single-family. very low density	781	11.31	23.76	1.47	1.32
Residential	D	variety of residential categories summarized in Table 3	1926	27.88	18.72	1.41	1.30
CBD	CBD	central business district - core activities of all types with a variety of related land uses	44	0.64	24.60	1.38	1.29
Commercial	C	includes office-buffer, high-intensity office/apartment, neighborhood commercial, thoroughfare service, and corridor commercial districts	2185	31.63	4.58	1.38	1.34
Hospital	HD	major hospital complexes and campuses	33	0.48	17.45	1.44	1.30
Industrial	I	variety of industrial uses including urban and suburban and light, medium, and heavy industry	498	7.21	22.12	1.51	1.32
Park	PK	permits all sizes and ranges of public park land and facilities, includes park peripheral areas assuring compatibility of adjacent land use	166	2.40	42.92	1.53	1.31
Airport	"A"	public airports municipally owned or operated, including all necessary navigation and flight operation facilities, and accessory uses	28	0.41	97.67	1.53	1.33

Note: A zoning GIS data layer was provided by Indianapolis Mapping and Geographic Infrastructure System, City of Indianapolis. Information on zoning category, code, and description were provided by Metropolitan Planning Department, City of Indianapolis. Other attributes in the table are computed and compiled by the authors. We also referenced to Wilson et al. 2003 in compilation of this table.

Relative LST is sufficient for mapping of the spatial variations of urban land surface temperatures. Therefore, the effects of atmosphere and surface roughness on LST were not taken into account in this study. Lack of atmospheric correction may introduce a temperature error of 4°C–7°C for the mid-latitude summer atmosphere [36]. The magnitude of atmospheric correction depends upon image bands used as well as atmospheric conditions and the height of observation. Errors due to urban effective anisotropy depend upon surface structure and relative sensor position, and can yield a temperature difference of up to 6 K or higher in downtown areas [36].

E. Statistical Analysis

Based on previous research results [20], [37], we hypothesized that the spatial variations of LST were related to four groups of factors that described LULC composition (six variables), biophysical conditions (four variables), intensity of human activities (four variables), and landscape pattern (four variables) (Table I). We computed the mean (and standard deviation) values of LST and each potential factor per general zoning polygon and per residential zoning polygon. Tables II and III show the definition for each zoning category and relevant attributes. Multiple stepwise regressions were then applied

TABLE III
RESIDENTIAL ZONING (POLYGON) ATTRIBUTES

Zoning category	Typical density (acre)	Primary use	Minimum open space	Typical lot size (sq. ft)	Comprehensive planning classification	Number of polygons	Percent of landscape	Mean polygon size (ha)	Mean shape index	Mean fractal dimension
DP	varies	planned unit development	varies	varies	varies	89	13.46	38.73	1.44	1.28
DS	0.5	suburban single-family	85%	1 acre	very low density	67	4.71	29.56	1.44	1.30
D1	0.9	suburban single-family	80%	24,000	very low density	104	4.61	20.07	1.37	1.29
D2	1.9	suburban single-family	75%	15,000	very low density	226	16.22	35.14	1.46	1.30
D3	2.6	low or medium intensity single-family	70%	10,000	low density	296	19.14	30.73	1.53	1.30
D4	4.2	low or medium intensity single-family	65%	7200	low density	195	10.95	26.99	1.48	1.30
D5	4.5	medium intensity single-family	65%	5000	low and medium density	231	19.74	33.35	1.56	1.32
D5II	5.0	medium intensity single- or two-family	65%	3200	low and medium density	17	D5II were merged into D5 for computing landscape metrics.			
D6	6– 9	low intensity multifamily	3.85	varies	medium density	81	5.10	12.44	1.36	1.28
D6II	9–12	medium intensity multifamily	2.65	varies	medium density	118	D6II were merged into D6 for computing landscape metrics.			
D7	12–15	medium intensity multifamily	2.10	varies	medium density	153	2.93	9.64	1.47	1.32
D8	5–26	urban multi-use residential	2.65	varies	high density	112	1.76	6.00	1.48	1.36
D9	12– 120	suburban high-rise apartment	0.29–1.45	varies	high density	29	0.34	5.68	1.35	1.33
D10	20– 140	central and inner-city high-rise apartment	0.27–1.18	varies	high density	9	0.04	1.43	1.23	1.33
D11	6.0	mobile dwellings	varies	Varies	medium density	23	0.93	22.40	1.34	1.26
D12	5.0	low-density two-family	65%	9000	low density	13	0.08	3.28	1.36	1.31

Note: See the Note to Table 2.

to obtain independent variables with statistical significances ($P < 0.001$). Variables that were removed from the stepwise regressions were not considered as the explanatory factors of LST variations and were, therefore, excluded in the subsequent statistical analyses. Next, factor analysis (specifically, principal component analysis) was conducted to transform the identified independent variables into a set of uncorrelated principal components. Factors whose eigenvalues greater than 1 were

TABLE IV
ROTATED FACTOR LOADING MATRIX FOR RESIDENTIAL ZONING, OCTOBER 3, 2000

Variables	Component 1	Component 2	Component 3	Component 4	Component 5
SHAPE_IN	0.035	0.022	0.883	-0.024	0.013
FRACTAL	-0.129	0.045	0.862	0.061	-0.115
LANDSIM	0.165	-0.202	0.021	0.052	-0.545
NDVI	0.963	-0.085	-0.038	0.063	-0.022
GV	0.875	-0.135	-0.066	0.175	-0.045
IMP	-0.613	0.654	-0.080	0.060	0.054
SOIL	-0.095	-0.877	-0.080	-0.118	-0.033
Per_Wa	-0.124	0.168	-0.027	-0.792	-0.023
Per_Ur	-0.876	0.213	0.058	0.247	0.057
Per_Fo	0.772	0.496	-0.017	-0.179	0.017
Per_Gr	0.193	-0.836	-0.042	0.157	-0.083
PAVEMENT	-0.327	0.327	0.016	0.530	-0.200
BLDG_ARE	-0.469	0.440	-0.011	0.460	0.230
POP_DEN	0.087	-0.086	-0.073	0.031	0.872
Initial Eigenvalues	4.41	2.17	1.61	1.23	1.07
% of Variance	31.521	15.521	11.489	8.764	7.668
Cumulative %	31.521	47.043	58.531	67.295	74.964

extracted [38], and the factor loadings of each original variable were examined.

F. Landscape Metrics Computation

Landscape pattern metrics have frequently been employed in landscape ecology to characterize the arrangement of species, communities, and habitat patches within landscapes [39]. Their potential for monitoring ecosystem changes and linking with ecological and environmental processes has been recognized [40]. These metrics can be applied to create quantitative measures of spatial patterns found on a map or remotely sensed imagery. When applying landscape metrics to remotely sensed data, each unique pixel value represents a patch type [39]. In this study, four landscape metrics were computed for each zoning polygon, including shape index of a zoning polygon, fractal dimension of a zoning polygon, landscape similarity index, and Shannon's diversity index of LULC composition within a zoning polygon. FRAGSTATS, a software program designed to compute a wide variety of landscape metrics for categorical map patterns, was selected for use [41]. The selection of these metrics was based on a research result by Riitters *et al.* [42]. Shape index, a simple measure of shape complexity, is computed by dividing patch perimeter by the minimum perimeter possible for a maximally compact patch of the corresponding patch area. In our study, patches refer to zoning polygons. Fractal dimension of a zoning polygon equals two times the logarithm of patch perimeter divided by the logarithm of patch area. A fractal dimension greater than 1 for a 2-D patch indicates an increase in shape complexity. Fractal dimension approaches 1 for shapes with very simple perimeters, and approaches 2 for shapes with highly convoluted, plane-filling perimeters. Fractal dimension index is appealing because it reflects shape complexity across a range of spatial scales. Similarity index equals 0 if all the patches within the specified neighborhood have a zero similarity coefficient, and increases as the neighborhood is increasingly occupied by patches with greater similarity coefficients and as those similar patches become closer and more contiguous and less fragmented in distribution. Shannon's diversity index equals 0 when the landscape contains only 1 patch (i.e., no diversity), and increases as the number of different patch types increases and/or the proportional distribution of area among patch types becomes more equitable.

IV. RESULTS

A. Factors Contributing to LST Variations

As a rule in interpreting factor analysis results, the suitability of data for factor analysis was first checked based on Kaiser–Meyer–Olkin (KMO) and Bartlett's test values [43]. Only when KMO was greater than 0.5 and the significant level of Bartlett's test was less than 0.1, the data was acceptable for factor analysis. The second step was to validate the variables based on the communality of variables. Among the eight PCA conducted (four for residential zoning and another four for general zoning), 11–14 variables finally entered into the factor analysis. Based on the rule that the minimum eigenvalue should not be less than 1, five factors were extracted from each factor analysis, with the exception of the general zoning of October 3, 2000, which had only four factors. Rotated factor loading matrices of residential zoning were generated for the four images. Table IV shows the loading matrix for the October image. Similarly, loading matrices for general zoning were produced for the four image. Table V shows the loading matrix of general zoning for the October image. From the residential zoning matrices, it became known that the first factor (factor 1) explained about 23%–35% of the total variance; the second factor (factor 2) accounted for 13%–15%, the third factor (factor 3) explained 11%–12%, the fourth factor (factor 4) 9%–10%, and the fifth factor (factor 5) 8%–9%. Together, the first five factors explained approximately 65%-80% of the variance. From the general zoning matrices, the first factor (factor 1) explained about 28%-36% of the total variance; the second factor (factor 2) accounted approximately for 12%, the third factor (factor 3) explained 9%–11%, the fourth factor (factor 4) 8%–9%, and the fifth factor (factor 5) about 7%. Overall, the first four/five factors explained between 61% and 73% of the variance.

TABLE V
ROTATED FACTOR LOADING MATRIX FOR GENERAL ZONING, OCTOBER 3, 2000

Variables	Component 1	Component 2	Component 3	Component 4
SHAPE_IN	0.064	0.065	0.846	0.195
FRACTAL	-0.051	-0.100	0.836	-0.212
LANDSIM	0.550	0.047	0.081	0.037
PAVEMENT	-0.258	-0.395	0.059	-0.397
MEAN_POP	0.263	0.013	-0.196	0.261
DIVERS	0.413	0.272	-0.027	0.539
PER_AG	-0.086	0.635	0.063	0.009
PER_WA	-0.142	-0.136	0.067	0.818
PER_FO	0.720	-0.323	-0.003	0.137
NDVI	0.944	0.060	-0.063	0.077
GV	0.894	0.043	-0.106	0.032
IMP	-0.733	-0.455	-0.040	-0.008
SOIL	0.105	0.865	-0.111	-0.002
Initial Eigenvalues	3.693	1.624	1.458	1.158
% of Variance	28.408	12.493	11.217	8.911
Cumulative %	28.408	40.900	52.118	61.028

Interpreting factor loadings is the key in factor analysis. Factor loadings are the measurement of the relationships between variables and factors. Generally speaking, only variables with loadings greater than 0.32 should be considered [43]. Comrey and Lee suggested a range of values to interpret the strength of the relationships between variables and factors [44]. Loadings of 0.71 and higher are considered excellent, 0.63 very good, 0.55 good, 0.45 fair, and 0.32 poor. When reading factor loadings on each variable for residential zoning, no matter which date of image is considered, Factor 1 always had strong loadings on the variables of biophysical conditions, including vegetation and impervious surface fractions, and NDVI. In most cases, Factor 1 also had a strong loading on the percentage of built-up land. Apparently, Factor 1 was associated with biophysical conditions. Factor 2 had a high loading on soil fraction for three images, except for the image of April 5, 2004, when Factor 2 had a strong positive loading on two landscape pattern variables (i.e., shape index and fractal dimension). Factor 3 showed high factor loadings either on population, landscape pattern variables, or percentage of water bodies. Similarly, Factor 4 displayed high loadings on different variables, such as percentage of water bodies, shape index, or percentage of agricultural land. Factor 5 had high factor loadings on population density, percentage of water bodies, and landscape pattern variables. Apparently, among Factors 3–5, one of the factors was associated with the percentage of water, the other with the landscape pattern variable(s), and still other, with population variable(s). In spite of slight differences, each factor explained approximate 10% of the total variance.

In viewing factor loadings for general zoning, Factor 1 was found to have a strong positive loading on vegetation fraction and NDVI for all of the four images (for the February and April images, strong positive loadings on percentage of grassland, too), while a strong negative loading on impervious surface fraction (also on percentage of built-up land for the June image). It may be concluded that regardless residential or general zoning, Factor 1 can be described as a biophysical conditions factor, and on average, explained 30% of the total variance in LST pattern. Factor 2 showed strong loadings on soil fraction, fractal dimension, or mean population. Factor 3 had a strong loading on landscape pattern variables, soil fraction, or percentage of forestland. Factor 4 held strong loadings on percentage of water for the three images, but had the strongest loading on shape index for the June image. Factor 5 possessed the strongest loading on the percentage of agricultural land for all images, with the exception of the October image, when this variable did not enter into the PCA.

B. Zoning Effect on LST: General Versus Residential Zoning

To assess the zoning effect on LST, the variance explained and the factor loadings of residential and general zoning of each image was examined. Results indicate that the cumulative variance accounted by all factors was always larger in residential zoning than that in general zoning. This finding suggests that factors contributing to the spatial variation of LST in the general zoning were more complex, or that the variables used for this study were more appropriate for explaining residential LST patterns. Regardless of the residential or general zoning, Factor 1 always had strong loadings (on average, 29% of the variance in residential zoning and 30% in general zoning) on the variables that described the biophysical conditions. These variables included vegetation fraction, impervious surface fraction, and NDVI. With a few exceptions, Factor 2 was found closely associated with soil fraction in both zoning schemes, another biophysical variable. These findings are consistent with most of the previous researches, pinpointing the correlation between the spatial pattern of LST and biophysical conditions in a specific region. Apparently, zoning, as a tool of urban planners, has a profound impact on the biophysical characteristics of urban landscapes by imposing such restrictions as maximum building height and density, the extent of impervious surface and open space, land use types and activities. These variables control surface energy exchange, surface and subsurface hydrology, micro- to meso-scale weather and climate systems in general and LST in particular [45].

Previous studies have proved that the spatial arrangement and areal extent of different LULC types regulate largely the variations of spectral radiance and texture in LST [2], [3], [19]. This study finds that the LULC composition variables generally played a less significant role in the spatial patterns of LST. However, the percentage of water bodies consistently

TABLE VI
PEARSON CORRELATION COEFFICIENTS BETWEEN LST AND LANDSCAPE METRICS IN THE RESIDENTIAL ZONING CATEGORIES

	MEAN_SIZ	SHA_INDE	AWMSI	FRACTAL	DLFD	AWMPFD
TS_M_00	-0.53	-0.04	-0.05	0.36	0.41	0.44
TS_S_00	-0.55*	-0.62*	-0.56*	0.16	0.39	-0.02
TS_M_01	-0.59*	-0.09	-0.04	0.46	0.48	0.50
TS_S_01	-0.56*	-0.65*	-0.55*	0.17	0.44	0.02
TS_M_04	-0.44	0.02	0.02	0.33	0.36	0.46
TS_S_04	-0.51	-0.62*	-0.53	0.17	0.37	-0.02
TS_M_06	-0.62*	-0.20	-0.07	0.57*	0.43	0.41
TS_S_06	-0.40	-0.35	-0.30	0.25	0.24	0.11

Note: Correlation is significant at the 0.01 level (two-tailed).
*Correlation is significant at the 0.05 level (two-tailed).
MEAN_SIZ: mean patch size;
SHA_INDE: mean shape index;
AWMSI: area-weighted mean shape index;
FRACTAL: fractal dimension;
DLFD: double log fractal dimension;
AWMPFD: area-weighted mean patch fractal dimension;
TS_M_00: mean land surface temperature, October 3, 2000.
TS_S_00: standard deviation of land surface temperature, October, 2000.

TABLE VII
PEARSON CORRELATION COEFFICIENTS BETWEEN LST AND LANDSCAPE METRICS IN THE NONRESIDENTIAL ZONING CATEGORIES

	MEAN_SIZ	SHA_INDE	FRACTAL	AWMSI	DLFD	AWMPFD
TS_M_00	-0.24	-0.11	0.02	-0.14	-0.29*	0.27
TS_S_00	0.24	0.09	-0.25	0.10	-0.03	-0.32*
TS_M_01	-0.21	-0.15	-0.02	-0.10	-0.43*	0.28*
TS_S_01	0.12	-0.04	-0.15	-0.03	0.04	-0.29*
TS_M_04	-0.24	-0.15	0.00	-0.17	-0.28*	0.27*
TS_S_04	0.28*	0.11	-0.26	0.14	0.04	-0.34*
TS_M_06	-0.06	-0.02	0.06	0.13	-0.31*	0.35*
TS_S_06	0.40*	-0.02	-0.23	0.04	-0.02	-0.26

Note: See the Note to Table 6.

had a strong impact on the LST variation of either residential or general zoning. While the percentage of built-ups was found highly correlated with the LST variation of residential zoning, both the percentage of forestland and agricultural land possessed an important influence on the LST variation in the general zoning. Therefore, statistical models may be built based on the composition of LULC types within a zoning unit, because the spatial arrangement and areal extent of different LULC types regulate largely the variations of spectral radiance and texture in LST [19]. Using a surface energy balance model, the spatial variations of LST may be modeled based on such factors as imperviousness, green vegetation coverage and abundance, and other biophysical variables, which have been identified to relate directly or indirectly to the radiative, thermal, moisture, and aerodynamic properties in the urban surface and subsurface [20]. This is because thermal spectral response for each pixel is largely controlled by the dynamic relationship among these biophysical variables. This dynamics would produce an aggregated effect on the surface energy balance for each zoning unit.

Population related variables, i.e., mean population and population density within a zoning polygon, had more explaining power in the spatial variation of residential zoning than that of general zoning. There was always a population related factor in the factor matrices of residential zoning. These factors accounted for the variance between 8% and 12%, when a population related variable was the single most important variable.

All factor loading tables indicate that the landscape metrics variables may play an important role in the LST spatial patterns. All the tables of factor loading matrices contained a factor that was mainly associated with the landscape metrics variable(s). The landscape pattern factors explained the variance ranging from 8% to 13%, with strong loadings on shape index and the fractal dimension of zoning polygons. In most cases, shape index contributed more to the landscape pattern factors than fractal dimension did. To further examine the relationship between LST and the landscape metrics of zoning polygons, the zoning polygons were grouped into categories (refer to Tables II–III). Mean and standard deviation values of LSTs were computed for each zoning category. Six metrics were calculated for the zoning categories, which included mean patch size, mean shape index, area-weighted mean shape index, mean fractal dimension, double log fractal dimension, and area-weighted mean patch fractal dimension. Table VI and VII show the results of correlation analysis between LST and landscape metrics in the residential and nonresidential zoning categories, respectively. For the residential zoning, mean patch size was found to negatively correlate with the standard deviation values of LST, implying that smaller zoning polygons tended to associate with larger temperature variations. Moreover, shape index and area-weighted shape index were both discovered to have a negative correlation with the standard deviation values of LST. That is to say, the more complex in shape a residential zoning category was, the more intrapolygon

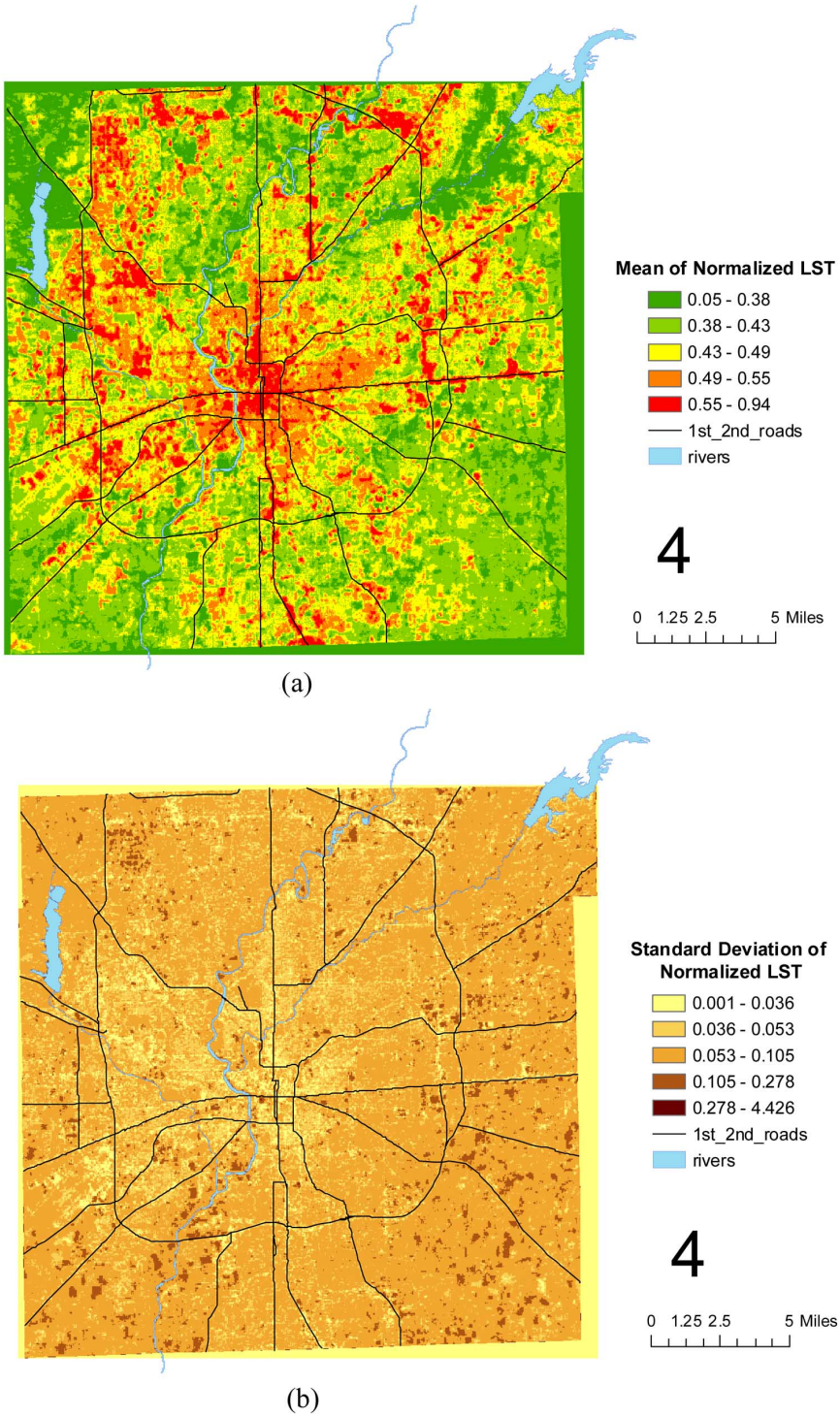

Fig. 2. Normalized land surface brightness temperatures computed based on the four dates of images. (a) Mean value of TN; (b) standard deviation values of $\mathrm{T_N}$.

variation of LST tended to be. Besides, fractal dimension and area-weighted mean patch fractal dimension values had a weaker positive correlation with the mean values of LST. In contrast, there was not any significant correlation found in the nonresidential zoning categories. The above observations should be viewed to be experimental. Further researches are warranted in the investigation of the relationship between the shape complexity of zoning polygons and the spatial variation of LST.

C. Seasonal Dynamics of LST Patterns

The ASTER images were taken in different seasons in different years. To compare and analyze these images together, normalized LST was computed according to following formula:

$$\mathrm{T_N} = \frac{\mathrm{LST} - \mathrm{LST_o}}{\mathrm{LST_s} - \mathrm{LST_o}} \tag{3}$$

where $\mathrm{LST_o}$ is the minimum value and $\mathrm{LST_s}$ the maximum value of LST in an image. As a result, the spatial pattern of LST

and T_N would be similar, however, all pixel values of T_N would be in the range of 0 to 1.

Fig. 2(a) shows the distribution of the mean of T_N values calculated from the images of four seasons. To show the spatial pattern better, major highways and water bodies were added to the map. This map has values ranged from 0.045 to 0.938 with a mean of 0.443 and standard deviation of 0.066. This choropleth map was produced based on Jenk's natural breaks classification scheme, in which classes were established among the largest breaks in the data array [46]. It is evident from the map that there was a thermal gradient as progressed from the Central Business District (CBD) out into the countryside. Some hot spots can be easily identified. The most extensive hot area was distributed in the central part of the city. Hot spots extended along Highway 465 (the by-pass of the city), in the north, west, and east side of the city, and became disconnected in the southern part of the city. Overall, a "hot ring" was evident from Fig. 2(a). Since urban development in Indianapolis took place along major radial transportation routes, "hot corridors" also existed along many highways that radiated from the city center. In contrast, vegetated areas, rivers and streams, and reservoirs detected low values of mean normalized LST.

Fig. 2(b) displays the standard deviation values calculated from the four images. This map shows the pixel-based spatial variability of T_N among the four seasons. It can be observed that LST fluctuated less in the central part of the city, especially in the CBD area, and the areas with extensive development, such as those along major highways. As we moved into the countryside, the values of standard deviation became larger. Numerous clusters of high standard deviations were clearly seen in the surrounding agricultural areas. In order to better understand the spatial variations of LST and to assess the environmental consequences of planning decisions, the standard deviation of T_N was computed for each general and residential zoning polygon. At the general zoning level, LST fluctuated most in dwellings (several types of residential categories—D), agriculture and single-family (DA), and parks (PK). In contrast, the low values of standard deviation, i.e., more steady LSTs throughout the year, were largely discovered in commercial uses (C), some of the low to medium single or multifamily residential (largely D5), and a few industrial zones (I). At the residential zoning level, the most pronounced LST fluctuation occurred in the planned unit development (DP), with some newly developed suburban single family (D2), low or medium intensity single-family housing (D3 and D4). Residential categories with least LST variability mainly included medium intensity single-family (D5), but can also be found in low or medium intensity multifamily (D6 and D7), low or medium intensity single-family (D4), urban multiuse residential (D8), and suburban high-rise apartment (D9). The vast majority of these residential polygons were located in the central part of the city, with few exceptions in the northern part of the city towards the Township of Carmel (a "bedroom" township for Indianapolis). It became clear that land use zones with less human activities generally possessed more notable seasonal variability in LST, regardless of referencing to general or residential zoning. On the other hand, zones with intensive human activities fluctuated less in LST. It can be hypothesized that anthropogenic heat, resulted from the use of air-conditioners, automobiles, and others, had a significant impact on the urban surface energy balance, leading to the reduction in the seasonal variability of LST.

V. Discussions and Conclusion

This study has examined the relationship between LST values and various GIS and remote sensing derived variables in Indianapolis, the United States. These variables can be grouped into four categories: LULC composition, biophysical conditions, intensity of human activities, and landscape pattern. Results indicate that the biophysical variables were most significant in explaining the spatial variations of LST, which included biophysical variables derived from SMA and NDVI. Regardless of the residential or general zoning polygons were examined, LST possessed a weaker relationship with the LULC compositions than with the biophysical variables. Principal component analysis further shows that one of the factors was associated with the percentage of water and the other with the landscape pattern variable(s). Population variables were found to be strong explanatory variables in the LST variability of the residential zoning, while the percentage of agricultural and/or forest land may be an explanatory variable for the general zoning.

Impervious surface coverage is an indicator of human activity intensity and has a great impact on urban surface energy exchange. GIS data layers of building footprints and pavements were obtained to create two imperviousness variables. However, the stepwise regression models for general zoning did not enter either variable. On the other hand, the regression models for residential zoning did enter one or both variables, with exception of the 2004 image. GIS-derived impervious surface variables did not contribute significantly to the principal components (loadings > 0.71). These variables may have correlated highly with some entered variables. It is also worthy to note that remotely sensed data and GIS data were collected with different formats. Remote sensing data had finer resolution than the GIS data. When integrating these two types of data, a common method is to aggregate remotely sensed data to an appropriate level of geographic entity, such as zoning polygons in this study. This aggregation has the potential to generate the same mean LST values in different zoning polygons in spite of their differences in biophysical conditions, LULC types, landscape pattern, and the intensity of human activities. This problem added to the difficulty in the analysis of urban LST variability.

The impact of land use zoning on urban biophysical conditions in general and LST in particular were further examined. Results show that the cumulative variance was always larger in residential zoning than that in general zoning, implying that the factors contributing to the LST variations in general zoning were more complex, or that the variables examined were more appropriate for explaining residential LST patterns. Our further investigation on the relationship between LST and the landscape metrics of zoning polygons suggests that for the residential zoning, smaller zoning polygons were associated with larger temperature variations, and that the more complex in shape a residential zoning category was, the more intrapolygon variation of LST tended to be. However, these correlations did not exist in the nonresidential zoning categories. Given the significance of landscape ecology in the understanding of LST patterns and processes and the implications of these findings in landscape design

and urban planning, more studies in this direction are called for. An interesting finding in this study is that Shannon' diversity index did not enter the stepwise regression models, so that it was not included in the consequent factor analysis. This is likely due to its close correlation with other variables.

The spatial pattern of LST in Indianapolis may be characterized as concentric in the central part of the city, a hot ring along the city's by-pass, and several hot corridors along the radial highways outward to the countryside. The seasonal fluctuation of LST was observed to be less in the central part, and increased towards the countryside. Numerous clusters of high LST fluctuation can be clearly identified in the surrounding agricultural areas, which alternated between a growing season and a dry, often plowed season, typical to many areas in the mid-western USA. At the general zoning level, LST fluctuated most in dwellings, agriculture and single-family, and parks, and least in commercial uses, a few low to medium single/multifamily residential, and industrial zones. While at the residential zoning level, LST fluctuated most in the planned unit development, but least in medium intensity single-family, low or medium intensity multifamily, low or medium intensity single-family, urban multiuse residential, and suburban high-rise apartment. In sum, zones with less human activities observed a strong seasonal LST variability, whereas zones with intensive human activities fluctuated less in LST. These findings may be interpreted in terms of the amount of anthropogenic heat emittance in different seasons. Apparently, the emittance of anthropogenic heat had a direct link with the reduction of the seasonal LST variability in Indianapolis. Whether this finding can apply to other mid-latitude cities in the northern hemisphere remain to be determined.

ACKNOWLEDGMENT

The authorswould like to thank two anonymous reviewers for their constructive comments and suggestions.

REFERENCES

[1] S. N. Goward, "Thermal behavior or urban landscapes and the urban heat island," *Phys. Geogr.*, vol. 1, no. 2, pp. 19–33, 1981.

[2] C. P. Lo, D. Quattrochi, and J. Luvall, "Application of high-resolution thermal infrared remote sensing and GIS to assess the urban heat island effect," *Int. J. Remote Sens.*, vol. 18, pp. 287–304, 1997.

[3] Q. Weng, "A remote sensing-GIS evaluation of urban expansion and its impact on surface temperature in the Zhujiang Delta, China," *Int. J. Remote Sens.*, vol. 22, pp. 1999–2014, 2001.

[4] J. A. Voogt and T. R. Oke, "Thermal remote sensing of urban climate," *Remote Sens. Environ.*, vol. 86, pp. 370–384, 2003.

[5] T. R. Oke, R. A. Spronken-Smith, E. Jauregui, C. S. B. Grimmond, and C. S. B. , "The energy balance of central Mexico City during the dry season," *Atmos. Environ.*, vol. 33, pp. 3919–3930, 1999.

[6] H. Tong, A. Walton, J. Sang, and J. C. L. Chan, "Numerical simulation of the urban boundary layer over the complex terrain of Hong Kong," *Atmos. Environ.*, vol. 39, pp. 3549–3563, 2005.

[7] A. Cendese and P. Monti, "Interaction between an inland urban heat island and a sea-Breeze flow: A laboratory study," *J. Appl. Meteorol.*, vol. 42, pp. 1569–1583, 2003.

[8] T. S. Saitoh, T. Shimada, and H. Hoshi, "Modeling and simulation of the Tokyo urban heat island," *Atmos. Environ.*, vol. 30, pp. 3431–3442, 1996.

[9] D. R. Streutker, "Satellite-measured growth of the urban heat island of Houston, Texas," *Remote Sens. Environ.*, vol. 85, pp. 282–289, 2003.

[10] X. Zhang, Y. Aono, and N. Monji, "Spatial variability of urban surface heat fluxes estimated form Landsat TM data under summer and winter conditions," *J. Agri. Meteorol.*, vol. 54, pp. 1–11, 1998.

[11] N. Chrysoulakis, "Estimation of the all-wave urban surface radiation balance by use of ASTER multispectral imagery and in situ spatial data," *J. Geophys. Res.*, vol. 108, 2003, DOI: 10.1029/2003JD003396.

[12] S. Kato and Y. Yamaguchi, "Analysis of urban heat-island effect using ASTER and ETM+ Data: Separation of anthropogenic heat discharge and natural heat radiation from sensible heat flux," *Remote Sens. Environ.*, vol. 99, pp. 44–54, 2005.

[13] Z. Bottyán and J. Unger, "A multiple linear statistical model for estimating the mean maximum urban heat island," *Theo. Appli.Clim.*, vol. 75, pp. 233–243, 2003.

[14] I. Eliasson, "Urban nocturnal temperatures, street geometry and land use," *Atmos. Environ.*, vol. 30, pp. 379–392, 1996.

[15] B. Dousset and F. Gourmelon, "Satellite multi-sensor data analysis of urban surface temperatures and landcover," *ISPRS J. Photo. Remote Sens.*, vol. 58, pp. 43–54, 2003.

[16] T. N. Carlson, R. R. Gillies, and E. M. Perry, "A method to make use of thermal infrared temperature and NDVI measurements to infer surface soil water content and fractional vegetation cover," *Remote Sens. Rev.*, vol. 9, pp. 161–173, 1994.

[17] R. R. Gillies, T. N. Carlson, J. Cui, W. P. Kustas, and K. S. Humes, "A verification of the 'triangle' method for obtaining surface soil water content and energy fluxes from remote measurements of the Normalized Difference Vegetation Index (NDVI) and surface radiant temperature," *Int. J. Remote Sens.*, vol. 18, pp. 3145–3166, 1997.

[18] K. P. Gallo and T. W. Owen, "Assessment of urban heat island: a multi-sensor perspective for the Dallas-Ft. Worth, USA region," *Geocartol. Inter.*, vol. 13, pp. 35–41, 1998.

[19] Q. Weng, D. Lu, and J. Schubring, "Estimation of land surface temperature-vegetation abundance relationship for urban heat island studies," *Remote Sens. Environ.*, vol. 89, pp. 467–483, 2004.

[20] T. R. Oke, "The energetic basis of the urban heat island," *Quart. J. Roy. Meteorol. Soc.*, vol. 108, pp. 1–24, 1982.

[21] D. Lu and Q. Weng, "Spectral mixture analysis of ASTER imagery for examining the relationship between thermal features and biophysical descriptors in Indianapolis, Indiana," *Remote Sens. Environ.*, vol. 104, no. 2, pp. 157–167, 2006.

[22] H. Fujisada, "ASTER level-1 data processing algorithm," *IEEE Trans. Geosci. Remote Sens.*, vol. 36, pp. 1101–1112, 1998.

[23] M. O. Smith, S. L. Ustin, J. B. Adams, and A. R. Gillespie, "Vegetation in Deserts: I. A regional measure of abundance from multispectral images," *Remote Sens. Environ.*, vol. 31, pp. 1–26, 1990.

[24] D. A. Roberts, G. T. Batista, J. L. G. Pereira, E. K. Waller, and B. W. Nelson, "Change identification using multitemporal spectral mixture analysis: applications in eastern Amazônia," in *Remote Sensing Change Detection: Environmental Monitoring Methods and Applications*, R. S. Lunetta and C. D. Elvidge, Eds. Ann Arbor, MI: Ann Arbor, 1998, pp. 137–161.

[25] J. F. Mustard and J. M. Sunshine, "Spectral analysis for earth science: investigations using remote sensing data," in *Remote Sensing for the Earth Sciences: Manual of Remote Sensing*, A. N. Rencz, Ed., 3rd ed. New York: Wiley, 1999, vol. 3, pp. 251–307.

[26] J. B. Adams, D. E. Sabol, V. Kapos, R. A. Filho, R. A. Roberts, D. A. Smith, M. O. , and A. R. Gillespie, "Classification of multispectral images based on fractions of endmembers: application to land cover change in the Brazilian Amazon," *Remote Sens. Environ.*, vol. 52, pp. 137–154, 1995.

[27] P. S. Chavez Jr., "Image-based atmospheric corrections—Revisited and improved," *Photo. Eng. Remote Sens.*, vol. 62, pp. 1025–1036, 1996.

[28] "ASTER Temperature/Emissivity Working Group. (1999). Temperature/Emissivity Separation Algorithm Theoretical Basis Document (version 2.4)," in JPL, California Institute of Technology. [Online]. Available: http://eospso.gsfc.nasa.gov/eos_homepage/for_scientists/atbd/docs/ASTER/atbd-ast-03.pdf [Online]. Available:

[29] A. Gillespie, S. Rokugawa, T. Matsunaga, J. S. Cothen, S. Hook, and A. B. Kahle, "A temperature and emissivity separation algorithm for advanced spaceborne thermal emission and reflection radiometer (ASTER) images," *IEEE Trans. Geosci. Remote Sens.*, vol. 36, no. 4, pp. 1113–1126, Jul. 1998.

[30] P. Dash, F. M. Gottsche, F. S. Olesen, and H. Fischer, "Land surface temperature and emissivity estimation from passive sensor data: Theory and practice—current trends," *Int. J. Remote Sens.*, vol. 23, pp. 2563–2594, 2002.

[31] T. Schmugge, A. French, J. C. Ritchie, A. Rango, and H. Pelgrum, "Temperature and emissivity separation from multispectral thermal infrared observations," *Remote Sens. Environ.*, vol. 79, pp. 189–198, 2002.

[32] F. Li, T. J. Jackson, W. P. Kustas, T. J. Schmugge, A. N. French, M. H. Cosh, and R. Bindlish, "Deriving land surface temperature from Landsat 5 and 7 during SMEX02/SMACEX," *Remote Sens. Environ.*, vol. 92, pp. 521–534, 2004.
[33] W. C. Snyder, Z. Wan, Y. Zhang, and Y.-Z. Feng, "Classification-based emissivity for land surface temperature measurement from space," *Int. J. Remote Sens.*, vol. 19, pp. 2753–2774, 1998.
[34] D. A. Artis and W. H. Carnahan, "Survey of emissivity variability in thermography of urban areas," *Remote Sens. Environ.*, vol. 12, pp. 313–329, 1982.
[35] B. L. Markham and J. K. Barker, "Spectral characteristics of the LANDSAT Thematic Mapper sensors," *Int. J. Remote Sens.*, vol. 6, pp. 697–716, 1985.
[36] J. A. Voogt and T. R. Oke, "Effects of urban surface geometry on remotely-sensed surface temperature," *Int. J. Remote Sens.*, vol. 19, pp. 895–920, 1998.
[37] T. R. Oke, "The urban energy balance," *Progr. Phys. Geogr.*, vol. 12, pp. 471–508, 1988.
[38] H. Kaiser, "The application of electronic computers to factor analysis," *Ed. Psychol.*, vol. 52, pp. 621–652, 1960.
[39] J. M. Read and N. S. N. Lam, "Spatial methods for characterising land cover and detecting land-cover for the tropics," *Int. J. Remote Sens.*, vol. 23, pp. 2457–2474, 2002.
[40] H. Li and J. F. Reynolds, "A simulation experiment to quantify spatial heterogeneity maps," *Ecology*, vol. 75, pp. 2446–2455, 1994.
[41] K. McGarigal, B. J. Marks, and B. J. Fragstats*, Spatial Pattern Analysis Program for Landscape Structure.*. Portland, OR: Dept. Agriculture, Forest Service, Northwest Research Station, 1995, p. 122.
[42] K. H. Riitters, R. V. O'Neill, C. T. Hunsaker, J. D. Wickham, D. H. Yankee, S. P. Timmins, K. B. Jones, and B. L. Jackson, "A factor analysis of landscape pattern and structure metrics," *Land Ecol.*, vol. 10, pp. 23–39, 1995.
[43] B. Tabachnick and L. Fidell*, Using Multivariate Statistics (Third edition)*. New York: Harper Collins, 1996.
[44] A. L. Comrey and H. B. Lee*, A First Course in Factor Analysis (Second Edition)*. Hillsdale, NJ: Lawrence Erlbaum, 1992, p. 423.
[45] J. S. Wilson, M. Clay, E. Martin, D. Stuckey, and K. Vedder-Risch, "Evaluating environmental influences of zoning in urban ecosystems with remote sensing," *Remote Sens. Environ.*, vol. 86, pp. 303–321, 2003.
[46] R. M. Smith, "Comparing traditional methods for selecting class intervals on choropleth maps," *Prof. Geogr.*, vol. 38, no. 1, pp. 62–67, 1986.

Qihao Weng (M'07) was born in Fuzhou, China, in 1964. He received the A.S. degree in geography from Minjiang University, China, in 1984, the M.S. degree in physical geography from South China Normal University in 1990, the M.A. degree in geography from the University of Arizona, Tucson, in 1996, and the Ph.D. degree in geography from the University of Georgia, Athens, in 1999.

He is currently an Associate Professor of geography and Director of the Center for Urban and Environmental Change, Indiana State University, Terre Haute. He is the author of more than 85 peer-reviewed journal articles and other publications. He has published the books *Urban Remote Sensing* (CRC, 2006) and *Remote Sensing of Impervious Surfaces* (CRC, 2007). He is also a series editor for *Taylor & Francis Series in Remote Sensing Applications*. His research focuses on remote sensing and GIS analysis of urban ecological and environmental systems, land-use and land-cover change, urbanization impacts, and human-environment interactions.

Dr. Weng is a member of ASPRS, AGU, and AAG. He serves as a national Director of the American Society for Photogrammetry and Remote Sensing (2007–2010) and the Secretary of the International Society for Photogrammetry and Remote Sensing Working Group VIII/1 (Human Settlement and Impact Analysis). He has been the recipient of the Robert E. Altenhofen Memorial Scholarship Award from the American Society for Photogrammetry and Remote Sensing (1999) and the Best Student-Authored Paper Award from the International Geographic Information Foundation (1998). In 2006, he received the Theodore Dreiser Distinguished Research Award from Indiana State University, the university's highest research honor bestowed to faculty. In 2008, he was awarded a senior fellowship from the NASA NPP program.

Hua Liu received the B.A. degree in computer-aided cartography from Wuhan Technical University of Surveying and Mapping, China, in 2000, the M.A. degree in cartography and GIS from Wuhan University in 2003, and the Ph.D. degree in physical geography from Indiana State University, Terre Haute, in 2007.

She is currently with the College of Arts and Letters, Old Dominion University, Norfolk, VA. Her research focuses on urban thermal behaviors, landscape pattern, and GIS and remote sensing applications in public health.

Bingqing Liang received the B.S. degree in geography eucation from South China Normal University, China, in 2002, and the M.A. degree in geography from Indiana State University, Terre Haute, in 2005. She is currently pursuing the Ph.D. degree at the Center for Urban and Environmental Change, Indiana State University.

Her research interest is the application of remote sensing and GIS to urban analysis at multiple scales, including urban temperature modeling, urban quality assessment, and residential population estimation.

Dengsheng Lu was born in China in 1965. He received the B.A. degree in forestry from Zhejiang Forestry University, China, in 1986, the M.A. degree in forestry from Beijing Forestry University, China, in 1989, and the Ph.D. degree in physical geography from Indiana State University, Terre Haute, in 2001.

He then worked in the Center for the Study of Institutions, Population, and Environmental Change and the Anthropological Center for Training and Research on Global Environmental Change, Indiana University, Bloomington, as a postdoctoral fellow and research scientist during 2001 and 2006. He is currently with the School of Forestry and Wildlife Sciences, Auburn University, Auburn, AL. His research focuses on land-use/cover change, biomass/carbon estimation, human-environment interaction, and urban impervious surface. He is the author of more than 40 peer-reviewed journal articles and book chapters.